A radio-frequency spin-polarized scanning tunneling microscope Ⓕ

J. Friedlein, J. Harm ⓘD, P. Lindner ⓘD, L. Bargsten, M. Bazarnik ⓘD, S. Krause ⓘD, and R. Wiesendanger ⓘD

COLLECTIONS

Ⓕ   This paper was selected as Featured

View Online   Export Citation   CrossMark

ARTICLES YOU MAY BE INTERESTED IN
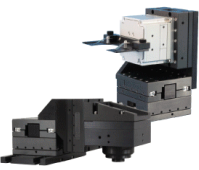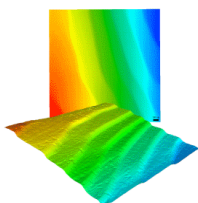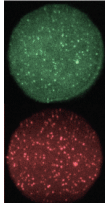
Upgrade of a low-temperature scanning tunneling microscope for electron-spin resonance
Review of Scientific Instruments **90**, 013706 (2019); https://doi.org/10.1063/1.5065384

Development of high-speed ion conductance microscopy
Review of Scientific Instruments **90**, 123704 (2019); https://doi.org/10.1063/1.5118360

Achieving low noise in scanning tunneling spectroscopy
Review of Scientific Instruments **90**, 101401 (2019); https://doi.org/10.1063/1.5111989

MCL MAD CITY LABS INC.
www.madcitylabs.com

Nanopositioning Systems

Modular Motion Control

AFM and NSOM Instruments

Single Molecule Microscopes

AIP Publishing

A radio-frequency spin-polarized scanning tunneling microscope (F)

View Online   Export Citation   CrossMark

J. Friedlein,[1,a] J. Harm,[1,a] (iD) P. Lindner,[1] (iD) L. Bargsten,[1] M. Bazarnik,[1,2] (iD) S. Krause,[1,b] (iD)
and R. Wiesendanger[1] (iD)

AFFILIATIONS

[1] Department of Physics, University of Hamburg, Jungiusstrasse 11, 20355 Hamburg, Germany

[2] Institute of Physics, Poznan University of Technology, ul. Piotrowo 3, 60-965 Poznan, Poland

[a] Contributions: J. Friedlein and J. Harm contributed equally to this work.
[b] Electronic mail: skrause@physnet.uni-hamburg.de

ABSTRACT

A scanning tunneling microscope for spin-resolved studies of dynamic systems is presented. The cryogenic setup allows the scanning tunneling microscope to achieve a cutoff frequency beyond 26 GHz at the tunnel junction and to be operable at temperatures of 1.1 K–100 K in a magnetic field of up to 3 T. For this purpose, the microscope and its wiring as well as the associated cryostat system were specially designed and manufactured. For sample preparation, an ultrahigh vacuum system was developed, which is equipped with modular preparation platforms. Measurements showing the characteristics of the scanning tunneling microscope in the time and frequency domain are presented. As a proof of concept, experimental data of the Pd/Fe/Ir(111) sample system at 95 K in a magnetic field of 3 T are presented.

Published under license by AIP Publishing. https://doi.org/10.1063/1.5104317

I. INTRODUCTION

Time-resolved measurements with spin-polarized scanning tunneling microscopy (SP-STM) led to numerous discoveries in the field of spin dynamics.[1–7] The switching of magnetic islands or clusters can be measured by recording and analyzing conductance changes observed as a telegraph noise signal. Yet, these measurements are limited by hardware constraints of conventional STM, as the required transimpedance amplifier (TIA) only has a bandwidth of several kilohertz at an amplifier gain of 10^8 A/V. In order to achieve a higher temporal resolution, techniques such as optical laser excitation[8–12] or RF-technology[13,14] have been utilized to enter the gigahertz range and beyond.

Spin dynamics experiments can also be performed by using electrical pump-probe methods.[15–17] However, for this, it is necessary to apply short voltage pulses to the tunnel junction. In contrast to ESR measurements, where a signal loss can be compensated by adjusting each frequency individually,[18] the whole frequency spectrum of a pulse has to be transmitted in pump-probe methods to overcome a broadening of the pulse width and pulse deformation, leading to a reduction in pump-probe time resolution.

The combination of RF-technology and cryogenics is challenging. Typical RF-cables have high electrical and thermal conductivity. Moreover, they are thick and rigid and cannot be bent strongly in order to avoid internal reflections and fractures in the insulation. Whereas short coaxial cables are advantageous in order to minimize signal losses in the RF-cabling, long cables with low thermal conductivity are desired for thermal decoupling of a cryogenic system from room temperature. Compromising between those factors is at heart of the described setup.

It enables dynamic SP-STM experiments on the picosecond time scale and an operation of the microscope in a temperature range of 1.1 K–100 K in an external magnetic field of up to 3 T in an ultrahigh vacuum (UHV) environment. In this setup, all-electrical signals are transferred to the tunnel junction for achieving a high temporal resolution. Therefore, the cryostat system is especially designed to maximize the RF-cabling bandwidth by allowing for a short RF-cable length while maintaining an easy tip and sample exchange utilizing rotatable isolation shields and supporting a holding time of the 4K stage of up to one week. For future usage options, optical viewports are provided to enable laser-based excitation at low temperatures.

II. MICROSCOPE DESIGN

The design of the radio frequency-STM (RF-STM) is depicted in Fig. 1. In this microscope, the tip side is optimized to deliver RF-signals to the tunnel junction. This was accomplished by using a semirigid cable for biasing the tip. The semirigid cable is fixed by two half pieces having a milling cut that exactly fits the semirigid cable radius for clamping and optimal cooling of the cable. Custom-made nonmagnetic Corning Gilbert G3PO connectors are used at the microscope stage. The tip side features an exchangeable female-female G3PO bullet that is modified with a press fitted aluminum ring. An *in situ* tip and sample exchange can be performed by utilizing a wobblestick. The wobblestick head is provided with hollow sections that can enclose the RF-connector and the aluminum ring to hold them for an exchange.

The concept of coarse movement is based on the Pan-design[19] and utilizes six piezostacks (PI Ceramic GmbH). In this microscope, the sample stage is moved by the coarse approach and is attached to a piezotube scanner (EBL Products, Inc.). This arrangement is commonly used in atomic force microscopes and was also used in the RF-STM by Saunus *et al.*[14,20] This configuration has the advantage in this setup that the stiff semirigid cable can be clamped to the microscope body. The sample, having a flexible non-RF coaxial cable, can be easily moved. For a sample exchange, the sample stage is brought into an exchange position. This fixes the sample stage and reduces the risk of breaking the tube scanner while exchanging the sample. The sample stage is glued to a Macor connector, which contains a spring that fixes the sample holder to the sample stage via a ruby ball. The Macor connector is glued to the tube scanner. The back side of the Macor connector is conical in shape. In the exchange position, the conus is tightly clamped to a pin mounted to the microscope body in order to absorb lateral forces on the tube scanner during a sample exchange. There is a 4 mm opening in the back of the microscope, which allows direct optical access to the tunnel junction by a laser.

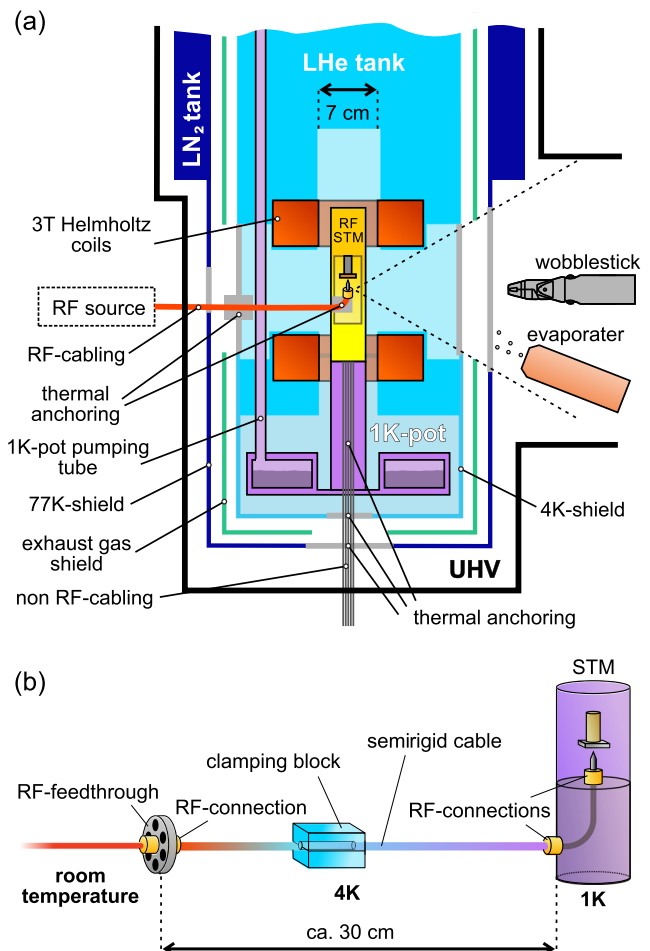The upper part of the STM body has been machined out of phosphor bronze, whereas the lower part has been made out of oxygen free copper (OFHC) for cryogenic reasons. The maximum diameter of the STM body is 39 mm.

III. CRYOGENICS AND CABLING

The cryostat system was developed in cooperation with CryoVac GmbH and is specially adapted to the needs of radio frequency cabling. A schematic drawing of the cryostat is given in Fig. 2(a). The system design allows for a cool down of the STM to a base temperature of 1.1 K using a 1K-pot while maintaining a RF-cable length of about 30 cm from room temperature to the 1K-stage. The 1K-pot can be directly filled from the liquid helium (LHe) main tank by opening a needle valve. The temperature reduction from 4.2 K to 1.1 K is achieved by pumping on the exhaust tube of the 1K-pot with a roots pump by Pfeiffer Vacuum GmbH, leading to a reduction in the vapor pressure at the surface of the 1K-pot.[21]

To isolate the STM from thermal radiation, isolation shields are mounted to the LHe tank and an additional liquid nitrogen (LN$_2$)

FIG. 1. Image and cross section of the RF-STM. The tip side is equipped with semirigid cabling and RF-connectors. Scanning and coarse approach is done on the sample side. *In situ* tip and sample exchange can be performed by using a custom-made wobblestick head.

FIG. 2. (a) Scheme of the cryostat. The LN$_2$-shield in dark blue, exhaust gas shielding in green, LHe shielding in light blue, and the 1K stage in purple. (b) Schematic of the RF-cabling from room temperature to 1 K. Clamping blocks ensure precooling at the LHe 4K bath.

tank, which can be partly opened and closed by a wobblestick. In addition, the exhaust gas from the evaporated helium of the main LHe tank is used for cooling an additional shield, placed between the LN_2 shield and the LHe shield, which benefits the LHe holding time. The LHe tank and the LN_2 tank dimensions are chosen in such a way to ensure a holding time of about one week with tank sizes of 130 l and 100 l, respectively.

Embedded in the LHe tank are superconducting Helmholtz coils, by which a 3 T magnetic field can be applied in an out-of-plane direction of the sample plane. The coils are always operated as a wet magnet. The 1K-pot with the STM is thermally well decoupled from the LHe system by thin walled stainless steel tubes. As a result, the 1K-pot cannot only be cooled down but also heated up to about 100 K by a resistive heater attached to the 1K-pot, with a small impact on the LHe holding time and without the risk of quenching the superconducting Helmholtz coils. This allows for an operation of the STM in a temperature range between 1 K and 100 K while operating in a magnetic field of up to 3 T.

The microscope is attached directly to the 1K-pot. For installation purposes, the cabling can be disconnected between the 4K stage and the 1K microscope body. The RF-wiring from the UHV-flange to the 1K-pot can be done through covers on the backside of the cryostat, i.e., on the opposite side of the wobblestick access. As depicted in Fig. 2(b), the RF-cable is clamped to the 4K stage between two OFHC clamping blocks that are attached to the LHe tank. They are mounted at the same height as the magnet and the cooling of the cables, and the corresponding damping of the cables is, therefore, independent of the LHe level in regular use. The installation of the RF-cable in between the Helmholtz coils allows for the optimal RF-cable length that is limited by the coil and isolation shield radii. A feedthrough (SMA45-FS-C16—MDC Vacuum Limited) with 2.92 mm connectors and a 45 GHz cutoff frequency rating is used for the connection to air.

For room temperature RF applications, silver-plated copper semirigid cables are a typical choice due to their high bandwidths. Since their thermal conductivity is very high, also at low temperatures, utilizing them between the 1K-pot and room temperature would lead to a drastic reduction in holding time of the cryostat. As a compromise, a semirigid coaxial cable made from beryllium copper with a silver-plated inner conductor was used (SC-119/50-SB-B—COAX CO, Ltd.). Beryllium copper offers the advantage of low thermal conductivity with relatively high electrical conductivity. Compared to systems with retrofitted RF-cabling, our design offers the advantage that the higher heat input acting on the cryostat and the STM stage has been compensated by a heat load adapted 1K pot and a larger tank size of the main LHe bath. The heat load acting on the 1K-pot and the 4K-bath was considered in calculations and simulations during the design process. Natterer *et al.* retrofitted their system with stainless steel RF-cabling with a long cable length of 1.5 m, as the holding time of the cryostat would otherwise have become too short to carry out measurements in a reasonable time scale.[13]

The 1K-pot can be operated in a continuous operation mode at base temperature while under a heat load of 5 mW. This is achieved by a capillary connecting the main helium tank with the 1K-pot for continuous refilling. In single shot mode, i.e., the 1K-pot with a volume of 1.2 l is filled and then decoupled from the main bath, a holding time of 4 weeks was achieved. The cable has an attenuation

of 6.3 dB/m at 20 GHz and 300 K and an attenuation of 2.2 dB/m at 20 GHz and 4 K. With the total length of the semirigid cabling of 35 cm from room temperature to the tip inside the STM, we estimated an attenuation of 1.5 dB at 20 GHz and 4 K, assuming a linear temperature gradient between room temperature and the 4K stage.

Maintenance of the microscope can be performed without lifting the cryostat by removal of the lower CF400 flange of the STM chamber. This flange gives access to covers below the cryostat where the STM wiring is fed through. An OFHC copper tube flanged to the 1K-pot is serving as a podest for the actual microscope parts. The copper tube is used to cool all the non-RF wiring being clamped to it. Wiring of the microscope was done using custom-made shielded twisted pair cables made out of 316L stainless steel, each with a thickness of 1 mm and covered with PFA. These cables were chosen because they offer robustness during installation with a minor impact on the holding time of the system. They are clamped to the 4K shield by a shielding plate and are loosely fed through the LN_2 stage.

IV. UHV SYSTEM

The UHV system includes two sample preparation chambers, the cryostat with an attached STM chamber, and a load lock. The layout of the UHV system is depicted in Fig. 3. The UHV system is mounted on an aluminum frame (Maschinenbau Kitz GmbH) being filled with sand for vibration damping. A decoupling of the whole system from building vibrations is achieved by passive damping legs with a resonance frequency of about 1 Hz (Integrated Dynamics Engineering GmbH). The setup is located in the basement to reduce the influx of building vibrations.

The chambers are equipped with scroll pumps (Edwards), turbomolecular pumps (Pfeiffer Vacuum GmbH), ion getter pumps
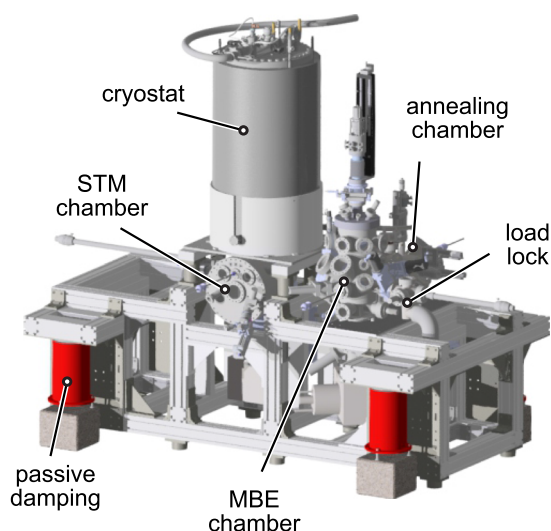
FIG. 3. Overview drawing of the UHV system. It has a load lock, MBE chamber, annealing chamber, and an STM chamber below the cryostat. The system is supported by an aluminum frame and is passively damped.

(Agilent Technologies, Inc.), and non-evaporable getter pumps (SAES Getters) for achieving UHV conditions ($<10^{-9}$ mbar). The whole system can be baked out by a custom-made bakeout tent (Hemi Heating AB). The bakeout tent is separated into two sections, which can be heated up to 150 °C individually from each other. By this, the preparation chambers can be baked out separately from the cryostat.

For sample preparation under UHV conditions, the system has two dedicated chambers, an annealing chamber and a chamber for molecular beam epitaxy (MBE). The annealing chamber includes an Ar^+ ion source (SPECS Surface Nano Analysis GmbH), a home-built electron beam stage,[20] and a resistive heating stage to clean the samples by ion bombardment and/or by heat. Furthermore, the samples can be heated up under low oxygen background pressures. Due to the separation into two preparation chambers, the MBE chamber can permanently stay under optimal UHV conditions and is not exposed to elevated pressures occurring during the crystal cleaning processes.

The MBE chamber is dedicated to growing thin films on the samples by molecular beam epitaxy. To this end, it includes several e-beam evaporators (FOCUS GmbH) and a low energy electron diffraction unit (SPECS Surface Nano Analysis GmbH), by which surfaces can be characterized. All active transfers in the chamber system are performed by the operation of wobblesticks that have a removable rail support for linear motion (Ferrovac GmbH). Magnetic transfer rods (MDC Vacuum Limited) are used for the passive transfers between the MBE chamber to the load lock or STM chamber.

The STM is mounted to the cryostat and can be accessed via a wobblestick from the STM chamber. Furthermore, the STM chamber is equipped with a storage facility for several tips and samples and an additional e-beam evaporator to deposit single atoms directly onto the cold sample surface inside the STM.

V. EXPERIMENTAL RESULTS

A. RF characterization

For testing the RF capabilities of the system, a vector network analyzer (VNA) and a cross correlation (CC) study were performed. To characterize the frequency response of the RF-cabling, a VNA measurement was done using a 26.5 GHz Agilent N5242A attached to the UHV feedthrough. The S11 component was measured to characterize the reflection of the RF-signal from the tunnel junction at the tip side (see Fig. 4). The STM was at a temperature of 4 K during the measurement and the tip separated by about 10 nm from the sample surface.

Since we are looking at a signal, which has been reflected at the tip and thereby travels twice through the RF-cabling, the cutoff frequency of the microscope is estimated to be located at −6 dB instead of −3 dB. It can be seen that the envelope of the signal is exceeding the measurement range of the VNA. In addition, sharp resonances at 7 GHz and 19 GHz appear, which could be caused by imperfect connections at the RF-connectors and/or an antenna effect of the tip. At 20 GHz, the reflection signal has an attenuation of about 3.5 dB (1.75 dB in one direction), which is in good agreement with our previous estimation of 1.5 dB, as additional attenuations through feedthroughs and connectors are likely to occur.
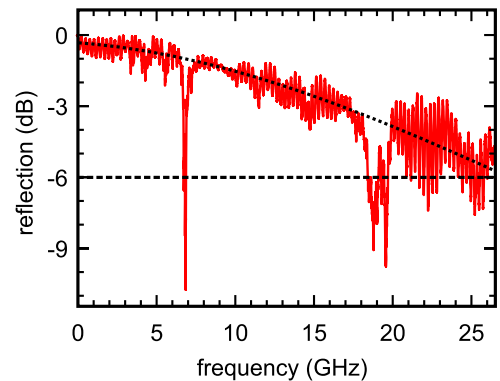

FIG. 4. Reflected RF-signal measured with a VNA, which shows the frequency characteristics of the RF-STM at a tip-sample distance of about 10 nm and a microscope temperature of 4 K. The envelope crosses the −6 dB line at over 26 GHz.

At elevated temperatures, the RF performance is expected to decrease only slightly, since the RF-cabling is permanently clamped to the 4K bath and only the RF-cable section from the tip to the 4K stage is heated up.

In addition, a cross correlation measurement was performed, which serves as a measure for the potential pump-probe time resolution. The wiring configuration for the cross correlation (CC) measurement is depicted in Fig. 5(a). For pulse generation, a Tektronix AWG70002A arbitrary waveform generator (AWG) was used with a Gaussian shape and a measured pulse length of 47 ps. The AWG has two channel outputs, CH1 and CH2. The AWG generates pulses on both channels of equal length (1 Sa) and height (250 mV) at a 25 GSa/s sampling rate with a 10% duty cycle. These channels can be skewed relative to each other by ± 100 ps on each channel, leading to a maximum delay time dt of ±200 ps between the pulses. The two outputs are added via a power combiner (Keysight 11636C DC to 50 GHz) to one signal, which is directly connected to the tip side of the tunnel junction. The current stabilized closed-loop feedback of the microscope was disabled during the cross correlation measurement. Now, the cross correlation scheme starts, where CH1 keeps a steady pulse pattern (P_{CH1}), whereas CH2 alternates between a pulse pattern (P_{CH2}) and a pattern without any pulses at an alternating frequency of 5 kHz. This alteration of the patterns is correlated with a reference modulation signal f_{mod} for the lock-in amplifier, which then can detect a change between the patterns at a particular delay dt between the channels. Through sweeping dt, the cross correlation of the pulses (CC) can then be reconstructed, which is presented in Fig. 5(b). It shows a Gaussian shape, which can be expected from the convolution of two Gaussian functions. This cross correlation peak has a full width at half maximum (FWHM) of 103 ps.

Since this measurement is limited by the AWG and the nonoptimized RF cabling used outside the UHV, the intrinsic time resolution of the system is expected to be better than this value. However, the FWHM of 103 ps shows that pump-probe measurements in the picosecond regime at low temperatures are feasible with this system. Thus, the possible temporal resolution is higher by a factor of 1000 compared to SP-STM systems without RF-cabling that only showed nanosecond time resolution.[15,16]
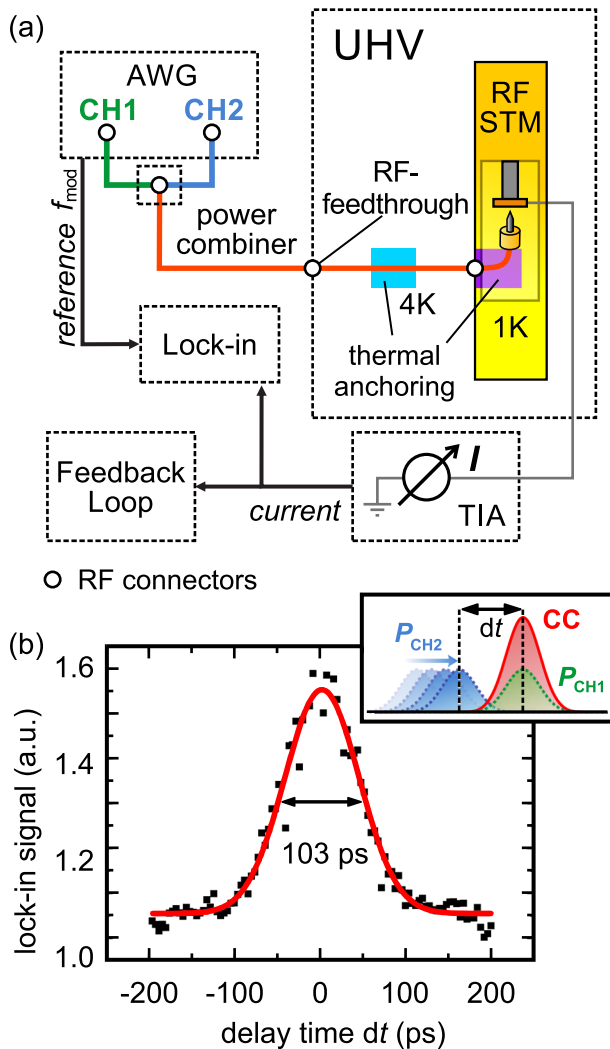
FIG. 5. (a) Wiring scheme for the cross correlation measurements. RF-cabling in red and regular cabling in gray. (b) Measured cross correlation (CC) on a Pd/Fe/Ir(111) sample system. CH1 of the AWG generates a pulse (P_{CH1}), which is being correlated with a shifting pulse of CH2 (P_{CH2}).

B. STM performance

In order to demonstrate the STM imaging capability, an Au(111) crystal was cleaned and examined. The sample preparation was performed in the annealing chamber by cycles of sputtering and annealing. Ar^+ ions with an energy of 1 keV were used for sputtering with a sputter current of 1 μA for 30 min. Afterward, the crystal was annealed on the resistance heating stage at a temperature of 500 °C. Sputtering was resumed 15 min after switching off the resistance heater with the crystal having a temperature of 160 °C at this point, as determined by a type K thermocouple. The sample was transferred into the STM at a base temperature of 1.1 K.
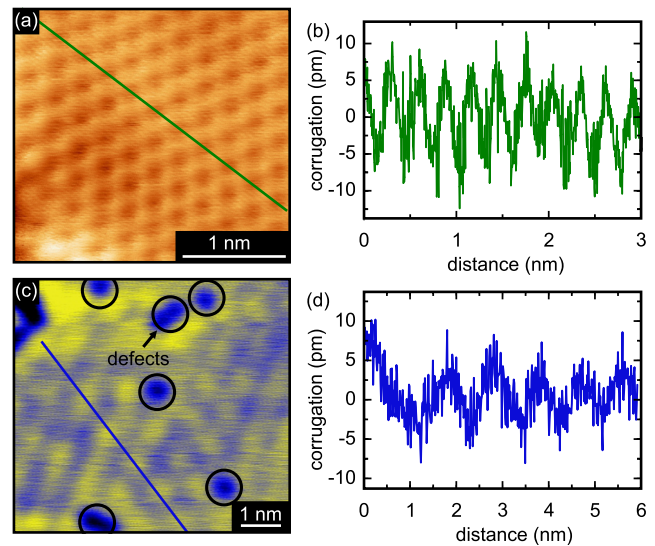
The atomic resolution on the Au(111) surface was successfully observed with a chromium bulk tip, as can be seen from the hexagonal atomic lattice in Fig. 6(a). From the line profile in Fig. 6(b), a corrugation of about 10 pm and an atomic lattice period of 0.28 nm are determined, which is in agreement with results of earlier studies.[22,23]

To demonstrate the capability of the microscope to perform SP-STM measurements, the Fe/Ir(111) nanoskyrmion lattice[24,25] was studied. Therefore, an Ir(111) crystal was cleaned in the annealing chamber using cycles of Ar^+ sputtering (U = 1 kV and I = 1 μA for 30 min) and O_2 annealing (10 min steps with temperatures of 1200 K, 1350 K, and 1500 K in the e-beam heater at 5×10^{-8} mbar absolute pressure). The Ir(111) crystal was flashed for 2 min at a temperature of 1500 K and transferred into the MBE chamber before Fe evaporation, which started 8 min after the flash. Fe was evaporated at a base pressure of 7×10^{-10} mbar. A chromium bulk tip was used as a scanning probe, which was glued to a G3PO bullet. For tip preparation, the tip was dipped into the iron layer to improve the magnetic SP-STM contrast.

Figure 6(c) shows an area of monolayer (ML) Fe on Ir(111), as resolved by SP-STM. This sample is known to exhibit a nanoskyrmion lattice with a period of about 1 nm.[25] Besides dark defects, a regular pattern is visible. The line profile in Fig. 6(d) shows a periodic corrugation with a period of about 1 nm and an amplitude of 10 pm. From previous SP-STM studies, it is known that the nanoskyrmion lattice can indeed exhibit a corrugation of about 10 pm. The microscope is, therefore, capable of performing sensitive SP-STM measurements.

The demonstration of the cross correlation temporal resolution and the SP-STM performance data shows that the microscope can be utilized for SP-STM experiments in the picosecond regime.

FIG. 6. (a) Topographical image with atomic resolution on an Au(111) surface: U = 100 mV, I = 1 nA, and T = 1.1 K. (b) Line profile along the green line depicted in (a). (c) SP-STM image of the Fe/Ir(111) nanoskyrmion lattice distorted by crystal defects: U = −50 mV, I = 8 nA, and T = 4 K. (d) Line profile along the blue line depicted in (c).
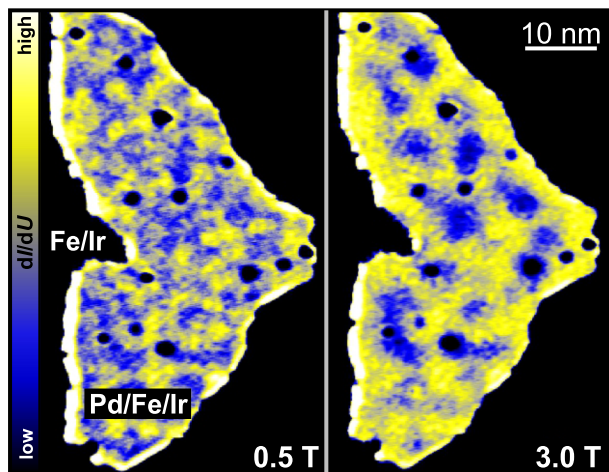
FIG. 7. dI/dU map of Pd/Fe nanoislands on Ir(111) at different magnetic fields imaged with NCMR contrast. Both images are taken at T = 95 K, I = 1 nA, and U = 700 mV. At B = 0.5 T, the islands show a disordered magnetic state. When the magnetic field is increased to B = 3 T, patches of noncollinear magnetization emerge.

C. Variable-temperature experiment

The operation of the microscope at variable temperatures in an external magnetic field of up to 3 T was first demonstrated based on a Pd/Fe/Ir(111) sample. The sample preparation of the Ir(111) crystal was done similarly to the above described preparation for the Fe/Ir(111) system. About 0.5 ML Fe and 0.2 ML Pd were deposited on the Ir(111) crystal at a sample temperature of about 200 °C during iron evaporation and 100 °C during palladium evaporation. The Pd/Fe/Ir(111) system is known to exhibit a spin-spiral phase at low temperatures in the zero magnetic field and can be driven into a skyrmionic phase by the influence of an external magnetic field.[26] The magnetic textures can be imaged using the noncollinear magnetoresistance (NCMR) effect in the Pd/Fe/Ir(111) system,[27] even when the tip is not spin-polarized. Figure 7 shows two dI/dU maps of a Pd/Fe/Ir(111) island taken at a sample temperature of 95 K at different magnetic fields. With a low magnetic field of 0.5 T, the island is in a disordered magnetic state, as indicated by irregular patterns. Increasing the external magnetic field to 3 T, the magnetization pattern of the island changes. Noncollinear spin-states emerge, which differ from the known circular shaped skyrmion appearances. By reducing the magnetic field, the effect is reversed again.

This measurement demonstrates the capability of the system to operate at temperatures up to 100 K with a magnetic field of up to 3 T.

VI. CONCLUSION

In summary, the design and first results of the RF-STM at temperatures of 1.1 K–100 K in a magnetic field of up to 3 T were presented. Atomic resolution on Au(111) has been achieved. It was shown that SP-STM experiments are feasible, as demonstrated by imaging the magnetic nanoskyrmion lattice on the Fe/Ir(111) sample system.

The RF characteristics of the setup have been studied, showing bandwidths above 26 GHz at 4 K. Finally, we have shown that our system is able to perform pump-probe experiments at cryogenic temperatures in the picosecond range by measuring a cross correlation with a FWHM of 103 ps.

REFERENCES

[1]M. Bode, O. Pietzsch, A. Kubetzka, and R. Wiesendanger, "Shape-dependent thermal switching behavior of superparamagnetic nanoislands," Phys. Rev. Lett. **92**, 067201 (2004).

[2]S. Krause, L. Berbil-Bautista, G. Herzog, M. Bode, and R. Wiesendanger, "Current-induced magnetization switching with a spin-polarized scanning tunneling microscope," Science **317**, 1537–1540 (2007).

[3]G. Herzog, S. Krause, and R. Wiesendanger, "Heat assisted spin torque switching of quasistable nanomagnets across a vacuum gap," Appl. Phys. Lett. **96**, 102505 (2010).

[4]S. Loth, S. Baumann, C. P. Lutz, D. M. Eigler, and A. J. Heinrich, "Bistability in atomic-scale antiferromagnets," Science **335**, 196–199 (2012).

[5]A. A. Khajetoorians, B. Baxevanis, C. Hübner, T. Schlenk, S. Krause, T. O. Wehling, S. Lounis, A. Lichtenstein, D. Pfannkuche, J. Wiebe, and R. Wiesendanger, "Current-driven spin dynamics of artificially constructed quantum magnets," Science **339**, 55–59 (2013).

[6]A. Spinelli, B. Bryant, F. Delgado, J. Fernández-Rossier, and A. F. Otte, "Imaging of spin waves in atomically designed nanomagnets," Nat. Mater. **13**, 782–785 (2014).

[7]M. Steinbrecher, A. Sonntag, M. dos Santos Dias, M. Bouhassoune, S. Lounis, J. Wiebe, R. Wiesendanger, and A. A. Khajetoorians, "Absence of a spin-signature from a single Ho adatom as probed by spin-sensitive tunneling," Nat. Commun. **7**, 10454 (2016).

[8]G. Nunes and M. R. Freeman, "Picosecond resolution in scanning tunneling microscopy," Science **262**, 1029–1032 (1993).

[9]S. Weiss, D. F. Ogletree, D. Botkin, M. Salmeron, and D. S. Chemla, "Ultrafast scanning probe microscopy," Appl. Phys. Lett. **63**, 2567–2569 (1993).

[10]W. Pfeiffer, F. Sattler, S. Vogler, G. Gerber, J.-Y. Grand, and R. Möller, "Rapid communication photoelectron emission in femtosecond laser assisted scanning tunneling microscopy," Appl. Phys. B: Lasers Opt. **64**, 265–268 (1997).

[11]O. Takeuchi, M. Aoyama, R. Oshima, Y. Okada, H. Oigawa, N. Sano, H. Shigekawa, R. Morita, and M. Yamashita, "Probing subpicosecond dynamics using pulsed laser combined scanning tunneling microscopy," Appl. Phys. Lett. **85**, 3268 (2004).

[12]S. Yoshida, Y. Aizawa, Z.-H. Wang, R. Oshima, Y. Mera, E. Matsuyama, H. Oigawa, O. Takeuchi, and H. Shigekawa, "Probing ultrafast spin dynamics with optical pump–probe scanning tunnelling microscopy," Nat. Nanotechnol. **9**, 588–593 (2014).

[13] F. D. Natterer, F. Patthey, T. Bilgeri, P. R. Forrester, N. Weiss, and H. Brune, "Upgrade of a low-temperature scanning tunneling microscope for electron-spin resonance," Rev. Sci. Instrum. **90**, 013706 (2019).

[14] C. Saunus, J. Raphael Bindel, M. Pratzer, and M. Morgenstern, "Versatile scanning tunneling microscopy with 120 ps time resolution," Appl. Phys. Lett. **102**, 051601 (2013).

[15] S. Loth, M. Etzkorn, C. P. Lutz, D. M. Eigler, and A. J. Heinrich, "Measurement of fast electron spin relaxation times with atomic resolution," Science **329**, 1628–1630 (2010).

[16] S. Krause, A. Sonntag, J. Hermenau, J. Friedlein, and R. Wiesendanger, "High-frequency magnetization dynamics of individual atomic-scale magnets," Phys. Rev. B **93**, 064407 (2016).

[17] S. Yan, L. Malavolti, J. A. J. Burgess, A. Droghetti, A. Rubio, and S. Loth, "Non-locally sensing the magnetic states of nanoscale antiferromagnets with an atomic spin sensor," Sci. Adv. **3**, e1603137 (2017).

[18] S. Baumann, W. Paul, T. Choi, C. P. Lutz, A. Ardavan, and A. J. Heinrich, "Electron paramagnetic resonance of individual atoms on a surface," Science **350**, 417–420 (2015).

[19] C. Wittneven, R. Dombrowski, S. H. Pan, and R. Wiesendanger, "A low-temperature ultrahigh-vacuum scanning tunneling microscope with rotatable magnetic field," Rev. Sci. Instrum. **68**, 3806–3810 (1997).

[20] H. von Allwörden, K. Ruschmeier, A. Köhler, T. Eelbo, A. Schwarz, and R. Wiesendanger, "Set-up of a high-resolution 300 mK atomic force microscope in an ultra-high vacuum compatible 3He/10 T cryostat," Rev. Sci. Instrum. **87**, 073702 (2016).

[21] F. Pobell, *Matter and Methods at Low Temperatures* (Springer-Verlag, New York, 1992), pp. 319.

[22] V. M. Hallmark, S. Chiang, J. F. Rabolt, J. D. Swalen, and R. J. Wilson, "Observation of atomic corrugation on Au(111) by scanning tunneling microscopy," Phys. Rev. Lett. **59**, 2879–2882 (1987).

[23] C. Wöll, S. Chiang, R. J. Wilson, and P. H. Lippel, "Determination of atom positions at stacking-fault dislocations on Au(111) by scanning tunneling microscopy," Phys. Rev. B **39**, 7988–7991 (1989).

[24] K. von Bergmann, S. Heinze, M. Bode, G. Bihlmayer, S. Blügel, and R. Wiesendanger, "Complex magnetism of the Fe monolayer on Ir(111)," New J. Phys. **9**, 396 (2007).

[25] S. Heinze, K. von Bergmann, M. Menzel, J. Brede, A. Kubetzka, R. Wiesendanger, G. Bihlmayer, and S. Blügel, "Spontaneous atomic-scale magnetic skyrmion lattice in two dimensions," Nat. Phys. **7**, 713–718 (2011).

[26] N. Romming, C. Hanneken, M. Menzel, J. E. Bickel, B. Wolter, K. von Bergmann, A. Kubetzka, and R. Wiesendanger, "Writing and deleting single magnetic skyrmions," Science **341**, 636–639 (2013).

[27] C. Hanneken, F. Otte, A. Kubetzka, B. Dupé, N. Romming, K. von Bergmann, R. Wiesendanger, and S. Heinze, "Electrical detection of magnetic skyrmions by tunnelling non-collinear magnetoresistance," Nat. Nanotechnol. **10**, 1039–1042 (2015).